Research Article Wiley Online Library ELECTROANALYSIS

doi.org/10.1002/elan.202200332

Physical Interpretation of Mixed Ionic-electronic Conductive Polymer-coated Electrodes by a Simple Universal Impedance Model

Marcel Tintelott[+],[a] Tom Kremers[+],[a] Anabel Mernitz,[a] Sven Ingebrandt,[a] Vivek Pachauri,[a] Xuan Thang Vu,[a] and Uwe Schnakenberg*[a]

Abstract: A simple equivalent electrical circuit is used to obtain the physical parameters of electrical circuit elements from measured electrochemical impedance spectra. This model consists of four circuit elements with a clear physical meaning for each of the elements. Compared to complex models with multiple constant phase elements or Warburg impedances, our model is suitable for extracting physical values for important electrode parameters with low errors. The feasibility of the model was shown by investigating pure metal or polymer-coated electrodes. Here, gold electrodes were coated either with Poly(3,4-ethylenedioxythiophene):poly(styrenesulfonate) (PEDOT:PSS), Polypyrrole:poly(styrenesulfonate) (PPy:PSS), or (PEDOT/PPy):PSS by means of electropolymerization. The model could demonstrate the ionic-electronic differences such as the ion accessibility of the differently coated electrodes. To prove the correctness of the model, the obtained results were compared to the literature.

Keywords: electrochemical impedance spectroscopy · liquid-solid interface · modeling · PEDOT:PSS · PPy:PSS

1 Introduction

Conjugated conductive polymers, like Poly(3,4-ethylenedioxythiophene)-poly(styrenesulfonate) (PEDOT:PSS) or Polypyrrole-poly(styrenesulfonate) (PPy:PSS), are gaining considerable attention in many applications due to their electrical and especially ionic-electronic properties, e.g., as organic electrochemical transistors [1], supercapacitors [2], organic light-emitting diodes [3], batteries [4], bioelectronic interfaces [5], biohybrid/artificial synapsis [6], pseudo-reference electrodes [7], and others [8]. Especially with regard to the ionic-electronic coupling, the coating of electrodes with conjugated polymers results in a significant lowering of the electrode impedance and in an increased charge injection capacity, which is of high interest for e.g. neural interfaces [9]. The coating of electrodes using conductive polymers can preferably be carried out by the electropolymerization technique. Here, a constant potential is applied to enable the electrochemical deposition process. The optimization of this process must be accompanied by suitable characterization techniques. One well-established method to investigate the electrode properties is the so-called electrochemical impedance spectroscopy (EIS) [7a,10]. Typically, a sinusoidal signal with an amplitude in the mV regime and a varying frequency is applied to the device under test to measure its frequency response. Here, the impedance spectra are commonly scanned from low ($\leq$10 Hz) to high ($\geq$1 MHz) frequencies. The obtained data contains information about the real and imaginary parts of the electrical impedance as a function of the frequency. Equivalent electrical circuits (EECs) can be utilized to translate the impedance data into valued electrical components and thus allowing the quantification or interpretation of the obtained data [7b,11]. The Randles circuit is probably the most known EEC to interpret EIS measurements [12]. Here, a solution resistance R_{SOL} in series with a double layer capacitance C_{DL} in combination with a Faradaic reaction impedance (based on a charge transfer resistance R_{ct} in series with a Warburg impedance Z_w) is used to describe the electrode/electrolyte interface. This EEC is, however, not suitable for all electrode/electrolyte systems. For instance, the charge transfer resistance R_{ct} can be extremely high in electrochemical systems where no Faradaic processes occur [7b]. Furthermore, the Randles circuit or modified versions are limited to a certain frequency range [7b,13]. Especially in the

[a] M. Tintelott,[+] T. Kremers,[+] A. Mernitz, S. Ingebrandt, V. Pachauri, X. T. Vu, U. Schnakenberg
Institute of Materials in Electrical Engineering 1, RWTH Aachen University, Sommerfeldstraße 24, D-52074 Aachen, Germany
E-mail: schnakenberg@iwe1.rwth-aachen.de

[+] These authors contributed equally.

Supporting information for this article is available on the WWW under https://doi.org/10.1002/elan.202200332

high-frequency domain, these types of models exhibit a large deviation from the measured EIS data. Therefore, EECs with multiple Warburg impedances and/or constant phase elements (CPEs) have been proposed to achieve better fitting of the EEC to the measured data [13–14]. However, the physical interpretation of these circuits is quite challenging. Therefore, a simple EEC with a clear physical correlation of the electronic components is of high interest for the interpretation and quantification of measured EIS data.

In this work, we propose a simple EEC to obtain relevant electrical parameters of different types of electrodes (e.g. bare metal or polymer-coated electrodes). The electrode/electrolyte interface is simply modeled by a solution resistance in series with a CPE. Parasitic effects from the measurement setup or the electrolyte are modeled using a resistance and a capacitance. To ensure a universal usage of this model, we validate the model to EIS spectra obtained from bare gold electrodes and gold electrodes coated with PPy:PSS, PEDOT:PSS, or (PEDOT/PPy):PSS, respectively. We compared the obtained information with the literature and used the film morphology of PEDOT:PSS and PPy:PSS to interpret the results.

2 Materials and Methods

2.1 Electrode Fabrication

Electrodes with a diameter of 500 µm were fabricated as described earlier [7a]. Briefly, a metal stack based on a 30 nm thick titanium (Ti) adhesion layer, 220 nm gold (Au), and 50 nm Ti as protective layer were sputter deposited on 4'' glass wafers. Subsequently, a 3.5 µm thick Parylene C layer was deposited as a dielectric layer. The circular electrode and the contact pads were opened by standard UV-photolithography followed by a reactive ion etching process. A schematic of the process flow is depicted in the supporting information (figure S1).

2.2 Polymer Coating

The electrodes were coated with PEDOT:PSS, PPy:PSS, or with a 1:1 mixture of both polymers. The monomer solutions (3,4-ethylene dioxythiophene (EDOT), pyrole (Py), and the PSS solution were purchased from Sigma-Aldrich Chemie GmbH, Taufkirchen, Germany. All solutions were dissolved in deionized (DI) water with a final concentration of 200 mM. Right before the polymer deposition process, the top protective Ti layer of the electrode was etched using ammonium hydroxide-hydrogen peroxide solution (ratio: NH_3 / H_2O_2/H_2O = 1/1/8) to obtain a clean Au surface [15]. The electropolymerization process was done by applying a voltage of 1 V vs. an equally-sized Au electrode using an EG&G Model 283 Potentiostat/Galvanostat (Princeton Applied Research, Oak Ridge, TN, USA). The fixed potential during the potentiostatic deposition was set to a value slightly above the oxidation potentials for all materials (0.6 V for pyrrole and around 0.9 V for EDOT). To ensure a reliable polymer deposition, the current was continuously monitored and integrated to obtain the deposited charge. The deposition process was terminated after a predetermined total charge was transferred. To further ensure highly reproducible coating results, a 3D-printed fluidic container with insertion slots for the working electrode (WE) and counter electrode (CE) were used [7a]. The PEDOT:PSS or PPy:PSS layer were obtained by electropolymerizing EDOT or Py and PSS (both 50 % v/v). The (PEDOT/PPy):PSS copolymer layer was realized by an EDOT (25 % v/v), Py (25 % v/v), and PSS (50 % v/v) mixture.

2.3 Impedance Spectroscopy Measurements

For EIS measurements, the bare gold or the coated electrodes served as the WE, while an Ag/AgCl pellet (Type EP2, World Precision Instruments, Inc., Sarasota, FL, USA) with a large surface area (by orders of magnitude larger than the WE to deliver enough current) was used as the CE, respectively. An electrochemical Ag/AgCl reference electrode (World Precision Instruments, Inc., Sarasota, FL, USA) was used as a reference electrode (RE). The impedance spectra were measured using a Novocontrol Technologies Alpha-A High-Performance Impedance Analyzer (Novocontrol Technologies GmbH & Co. KG, Montabaur, Germany). The impedance spectra were measured in a wide frequency range (from 0.1 Hz to 1 MHz), with an applied voltage amplitude of 10 mV in phosphate-buffered saline (PBS) electrolyte (pH 7.4) (Sigma-Aldrich Chemie GmbH, Taufkirchen, Germany).

2.4 Equivalent Electrical Circuit

The EEC used in this study is shown in Figure 1. This model is derived from a modified Randles EEC. Here, the electrode/electrolyte interface is modeled by a constant phase element (CPE_{DL}) in series with the resistance of the solution R_{SOL} [16]. The impedance of the CPE_{DL} is defined as $Z = 1/[Q^*(j\omega)^n]$ [17] to ensure proper matching of the model to the obtained data in the high-frequency region. Parasitic effects are subsumed by a capacitor and a resistance C_{PAR} and R_{LEAD}. C_{PAR} represents mainly the

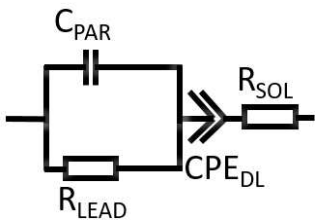

Fig. 1. Proposed EEC to model the EIS spectra. A serial combination of R_{SOL} and CPE_{DL} is used to model the electrode/electrolyte interface. Parasitic effects are included using the capacitance C_{PAR} parallel with the resistance R_{LEAD}.

wiring of the setup and the dielectric properties of water. At high frequencies, the ions in the buffer solution cannot follow the electric field. Thus, PBS is electrically behaving like deionized water. R_{LEAD} included contributions of cables, feed lines, and Ohmic contributions of the electrode itself. All EIS data were fitted using the Powell algorithm (500 iterations) and the open-source software "EIS Spectrum Analyser" [18].

3 Results and Discussion

3.1 Electrical Measurements

Figure 2 shows Bode plots for all types of electrodes (PEDOT:PSS, PPy:PSS, (PEDOT/PPy):PSS, and bare Au). The polymer-coated electrodes were obtained by electropolymerization with a total deposition charge of 700 µC. The transferred charge was a result of the polymerization process and, therefore, ensured a controlled amount of the deposited polymer as shown in a former study [7b]. The film thicknesses, which can be seen in figure S2 and S3, were in the range from a few tens of nm (for low deposition charges) up to above 1 µm (for high deposition charges). All electrodes exhibited a typical capacitive behavior in the low-frequency regime (<100 Hz) and a resistive behavior at higher frequencies (>1 kHz). Compared to bare noble metal electrodes, the deposition of polymers or the polymer mixture resulted in a broader resistive plateau and an overall lower impedance in the capacitive regime at low frequencies. The lowering in interfacial impedance due to polymer coatings is a well-known effect [7a]. The direct comparison of the differently polymer-coated electrodes furthermore reveals significant differences. The PEDOT:PSS electrode showed the largest gradient in the capacitive regime, while the PPy:PSS electrode exhibited the lowest gradient in the low-frequency regime (Figure 2; n-values obtained from the EEC shown in Figure 1). The mixed (PEDOT/PPy):PSS electrode showed an in-between behavior. At frequencies below 10 Hz, the impedance seems to follow the behavior of a PEDOT:PSS electrode, while it approached the behavior of a PPy:PSS electrode for increasing frequencies. Furthermore, the data reveals that the PEDOT:PSS electrode exhibited an increased capacitive behavior compared to the other electrodes in the lower frequency region. This capacitive behavior is not correlated to the actual capacitance value of the electrode, but to the steepness of the curve, respective the maximum phase shift in the low frequency regime of the Bode plot, as depicted by the dotted lines in Figure 2. Here, the phase diagram provides clear evidence. A PEDOT:PSS electrode approached a phase shift of almost −90°. In comparison, a PPy:PSS electrode exhibited a maximum phase shift of around −70°, while the phase shift of a (PEDOT/PPy):PSS electrode with around −80° was in-between. The corresponding different slopes in the low-frequency region are the reason for the crossing of the PEDOT:PSS EIS spectrum and (PEDOT/PPy):PSS spectrum at frequencies below 1 Hz.

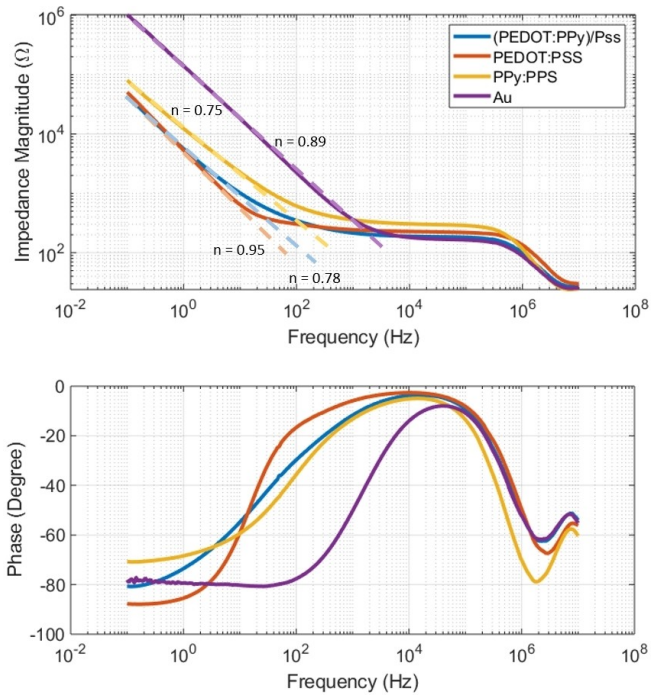

Fig. 2. Bode plots for three types of polymer-coated electrodes (all deposited with a total deposition charge of 700 µC) and a bare gold electrode as comparison. EIS measurements were performed in PBS in a standard 3-electrode setup using an Ag/AgCl pellet as CE, an Ag/AgCl electrochemical reference electrode as RE, and the electrode under test as WE.

To get a deeper insight into the different electrode properties, bare gold electrodes were coated with deposition charges of 10 µC, 100 µC, 250 µC, and 550 µC, respectively. The corresponding Nyquist plots are shown in Figure 3. Here, clear differences in the electrode properties due to the growth of thicker polymer films can be seen. All PEDOT:PSS coated electrodes exhibited a similar semicircle for all deposition charges but showed a clear difference in the lower frequency range. Therefore, it can be concluded that the electrode resistance of PEDOT:PSS coated electrodes does not change with increasing film thickness. However, eventually lower ion mobility inside the porous electrode coating and the capacitive behavior of the electrical double layer are both scaling with the growth of the PEDOT:PSS layer. With increasing film thickness, respectively with an increasing deposition charge, the PEDOT:PSS electrode exhibited a more capacitive behavior than the others. The PPy:PSS electrodes, however, showed an increasing semicircle with an increasing deposition charge. Furthermore, the changing steepness in the low-frequency regime of the Nyquist plot reveals that a PPy:PSS electrode has a reduced capacitive behavior with increased polymer film thickness. The (PEDOT/PPy):PSS electrode, again, exhibited behavior in between the two polymers. On the one hand, the electrodes showed a lower increase in the semicircle

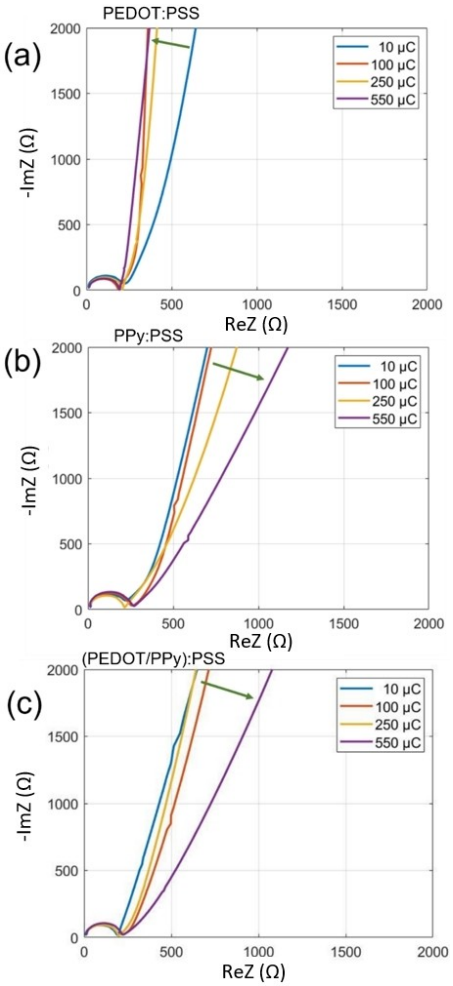

Fig. 3. Nyquist plots for the differently coated electrodes: (a) The PEDOT:PSS electrodes exhibited a higher capacitive behavior with increased deposition charge. (b) PPy:PSS electrodes exhibited a lower capacitive behavior and an increasing resistance with increased deposition charge. (c) (PEDOT/PPy):PSS electrodes exhibited an decreased capacitive behavior and a rather constant semicircle with increased deposition charge.

diameter compared to PPy:PSS electrodes with increasing polymer film thickness. The (PEDOT/PPy):PSS electrode reveals a more capacitive behavior compared to a PPy:PSS electrode and a less capacitive one compared to PEDOT:PSS electrodes. The arrows in Figure 3 indicate the directional change in the low-frequency regime and, therefore, the change in the capacitive behavior of the electrode.

3.2 Modeling the Electrode Properties

We introduce a simple EEC, as depicted in Figure 1, which contains only a few circuit elements and thus allows an easy interpretation and quantification of the electrode properties over the entire investigated frequency range. In a previous study, we have shown that the model according to Schöning et al. and Ende et al. exhibits limitations in the high-frequency domain of the impedance spectra [7b,19].

Figure 4 exemplarily shows the measured and fitted impedance magnitudes in dependence of the frequency for a bare Au electrode and the three different polymer-coated electrodes. The deposition charges of the PEDOT:PSS, PPy:PSS, and (PEDOT/PPy):PSS, were 550 µC, 700 µC, and 250 µC, respectively. These randomly chosen electrodes were used to demonstrate the good fitting quality for all kinds of electrodes of our proposed model. In Table S1 (supporting information) we summarized the values of the different circuit elements. As shown in Figure 4, the fitted curves exhibit a good agreement with the measured data over the whole simulated frequency range. The physical values of the CPE_{DL} were found to be $Q(CPE_{DL}) = 1.41\ \mu Fs^{(n-1)}$ ($\pm 0.63\,\%$) and $n(CPE_{DL}) = 0.89$ ($\pm 0.12\,\%$) for a bare Au electrode, respectively. The bulk electrolyte resistance R_{SOL} was determined to be 11 Ω ($\pm 6.63\,\%$). The low electrolyte resistance can be attributed to the large cross-section of the fluidic setup and the high ionic strength of the electrolyte. The capacitance C_{PAR} and resistance R_{LEAD} were found to be 1.68 nF ($\pm 1.66\,\%$) and 157.1 Ω ($\pm 0.89\,\%$), respectively. In Figure 4, it can be seen that the proposed model exhibits a good agreement with all measured EIS spectra.

Table 1 shows the obtained circuit element values for the different polymer-coated electrodes. The used model is very well suited to determine the electrical circuit elements with extremely low errors.

In the next step, the impedance spectra of thirty different electrodes (Au, PEDOT:PSS, PPy:PSS, and (PEDOT/PPy):PSS) were measured as described before to investigate the reliability of the proposed model. In

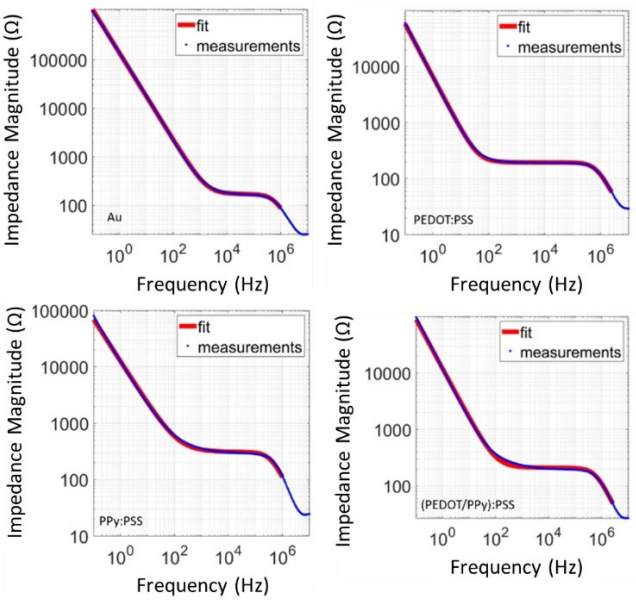

Fig. 4. Measured EIS data and the corresponding fittings using the proposed model for four types of characterized electrodes.

Table 1. The physical values and the respective fitting errors for the circuit elements of the EEC were obtained by the Powell algorithm using the software "EIS Spectrum Analyser".

	R_{SOL} [Ω]	R_{LEAD} [Ω]	$Q(CPE_{DL})$ [$\mu Fs^{(n-1)}$]	$n(CPE_{DL})$ [1]
PEDOT:PSS	11.72	183.9	0.26	0.95
(550 µC)	(±7.18 %)	(±0.64 %)	(±0.77 %)	(±0.24 %)
PPy:PSS	1.96	306.9	0.2	0.75
(700 µC)	(±88.44 %)	(±1.36 %)	(±1.45 %)	(±0.48 %)
(PEDOT/PPy):PSS	12.53	174.1	0.25	0.87
(250 µC)	(±13.65 %)	(±1.72 %)	(±1.88 %)	(±0.59 %)

order to do so, the obtained values for the parasitic circuit elements were compared. The mean value for the parasitic capacitance C_{PAR} was found to be 1.35 nF (±0.22 nF). Since the same experimental setup was used to measure the impedance spectra of all electrodes, only small variations in the parasitic capacitance are expected and proved by our model. Hence, the value for C_{PAR} is not shown in Table 1. The relatively large variation of R_{LEAD} is the result of the fitting algorithm to obtain the best overall fitting quality. Since the contribution of this circuit element is rather low with respect to the overall impedance, it was adjusted to obtain the overall lowest error of the fits. In addition, the PPy:PSS electrodes showed an increasing electrical resistance with increasing film thickness. For example, a PPy:PSS electrode coated with a deposition charge of 10 µC showed a lower electrode resistance compared to an electrode coated with a deposition charge of 250 µC, which is already known from our previous study [7b]. This can be explained by the increasing density in the PPy:PSS bulk film and the resulting decrease in ionic conductivity. Therefore, this dense area of the polymer coating can be electrically interpreted as an additional resistor.

To further investigate the ability of our model to determine the physical parameters of different polymer-coated or bare Au electrodes, all circuit elements were extracted from the thirty EIS spectra and plotted with regard to the deposition charge for all polymer coatings, as shown in Figure 5. The double-layer capacitance $Q(CPE_{DL})$ increased almost linearly with increasing film thickness (or deposition charge) for the PEDOT:PSS coated electrodes. The n value of the CPE_{DL} indicates that PEDOT:PSS coated electrodes exhibited an almost perfect capacitive behavior. Here, the n value was constant (~0.95) with deposition charges larger than 70 µC. The PPy:PSS coated electrodes, by contrast, exhibited an increasing capacitance until a deposition charge value of 400 µC and saturated for higher deposition charges. The n value indicates that a PPy:PSS coated electrode exhibited a less capacitive behavior compared to the PEDOT:PSS coated electrodes, which was also decreasing with increasing deposition charge before it saturated at around 0.75. The polymer composite (PEDOT/PPy):PSS exhibited a similar capacitance compared to the PPy:PSS coated electrodes for deposition charges

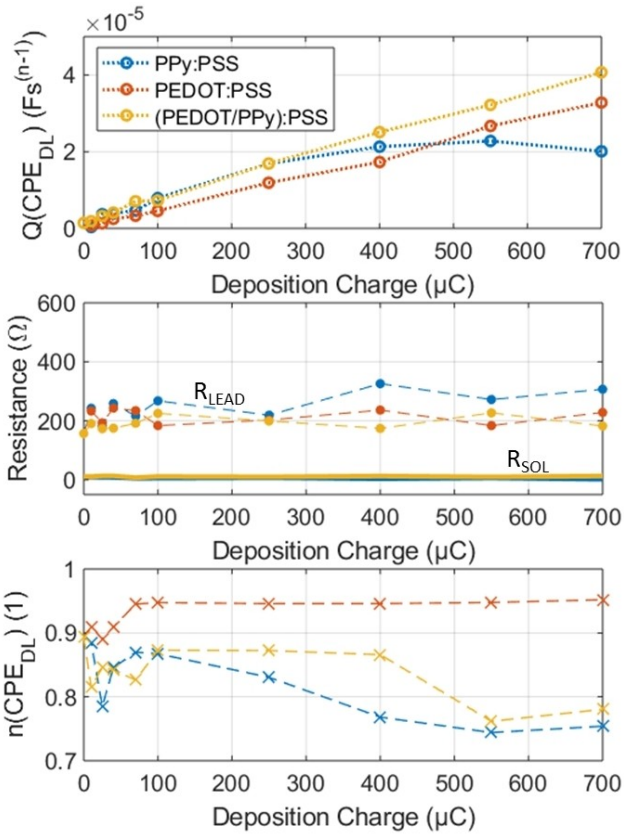

Fig. 5. Evolution of the physical parameters for different deposition charges of the electropolymerization process. A deposition charge of 0 µC represents a bare gold electrode. All parameters were obtained from the fitting of the EIS spectra to the proposed model as depicted in Figure 1.

lower or equal to 250 µC. In contrast to the PPy:PSS coated electrodes, the (PEDOT/PPy):PSS coated electrodes showed an increasing capacitance similar to the PEDOT:PSS electrodes for higher deposition charges. The modeled solution resistance R_{SOL} was rather constant for all simulated electrodes, which also makes sense since the experimental conditions in terms of distance between the electrodes and the electrolyte conductivity were kept constant. The lower solution resistance R_{SOL} for the PPy:PSS (700 µC) can be explained by either larger electrolyte volume and therefore, a lower electrolyte resistance, or by small differences in the PBS preparation. The high error can be attributed to the low resistance value and is, therefore, acceptable. However, the overall low R_{SOL} values indicate that the impact of the solution resistance is negligible in our measurement setup. These experimental data confirmed that with our proposed model, highly reliable simulation results can be obtained. The resistance value R_{LEAD} remained almost the same for all characterized electrodes as well. As already mentioned, the different parameters were adjusted to obtain the minimum error between the fitted EEC model and the measured spectra. Therefore, the fluctuation of the R_{LEAD} values is a result of the numerical optimization

process during fitting. Since the resistance value of R_{LEAD} is rather small and does not have a high impact on the overall impedance, the adjustment of this value results in a large error for the single element, but in a low error with respect to the total impedance. Only a slightly increasing trend can be observed for the PPy:PSS coated electrodes. This effect, however, matches with previously obtained simulation results for the PPy:PSS coated electrodes. The hypothesis is that an increasing PPy:PSS layer thickness results in an increase in the electrode resistance [7b].

To verify the obtained information based on the proposed EEC, we compared our findings to the state-of-the-art literature. For PEDOT:PSS it is well understood that the material exhibits an intrinsic volumetric capacitance [20]. Based on a 1D and 2D Nernst-Planck-Poisson modeling approach in combination with experimental results it could be demonstrated that this capacitance originated from the electrical double layer (which was formed along with the interface between PEDOT-rich and PSS-rich grains) [20]. Therefore, the electrical double layer capacitance increased with larger film thickness due to a higher amount of nanoscale PEDOT-rich and PSS-rich grain interfaces. Furthermore, it was shown that the intrinsic capacitance of the PEDOT:PSS coated electrodes increased with a linear trend until a saturation plateau was reached above a critical volume [21]. The electropolymerization of PEDOT:PSS results in the growth of a highly porous and highly accessible layer, while PPy:PSS exhibits denser films with low ion accessibility to a thicker layer [13,21b,22]. Taking the growth mechanisms of the two investigated polymers (PPy:PSS and PEDOT:PSS) into account, our model is suitable to explain their physical growth and the quantification of physical electrode parameters. The morphological differences between an Au electrode, PEDOT:PSS, and PPy:PSS coated electrodes are illustrated in Figure 6. PEDOT:PSS is highly accessible for ions and, therefore, an increasing capacitance with increasing deposition charge can be modeled. The increasing modeled capacitance value is in excellent agreement with the literature [20–21]. The increasing thickness of a PEDOT:PSS film results in a larger volumetric PEDOT-rich and PSS-rich interface and thus in a higher double-layer capacitance. In contrast to the highly porous PEDOT:PSS layer, a PPy:PSS layer exhibits a much denser structure. Therefore, the accessibility of the bulk polymer is not given and the capacitance remains constant once a critical thickness is reached. At the beginning of the polymerization process, a PPy:PSS with (a normally) higher surface roughness is obtained [23]. Due to the surface roughness and the volumetric capacitance of the PPy:PSS film, an increasing double layer capacitance is expected and modeled. However, during the polymerization process, the porous cavities deep in the bulk of the film are closed and are therefore not accessible for ions and a capacitance saturation is obtained [24]. This effect can also be proven by investigating the parasitic resistance of PPy:PSS coated electrodes. While the other electrode types exhibited a constant parasitic resistance, the PPy:PSS electrodes showed an increasing trend. This trend can be explained by the increasing layer thickness of the denser, non-accessible PPy:PSS bulk. This effect was already shown by Snook and Best [13]. They investigated the co-deposition of PPy and PEDOT in an ionic liquid at room temperature. Their results match our results. While the capacitance of a PPy electrode is saturating, a PEDOT and (PEDOT:PPy) coated electrode exhibited an increased capacitance of the investigated deposition charge. Since our study was performed using PEDOT and/or PPy combined with PSS, small differences in the results can be expected.

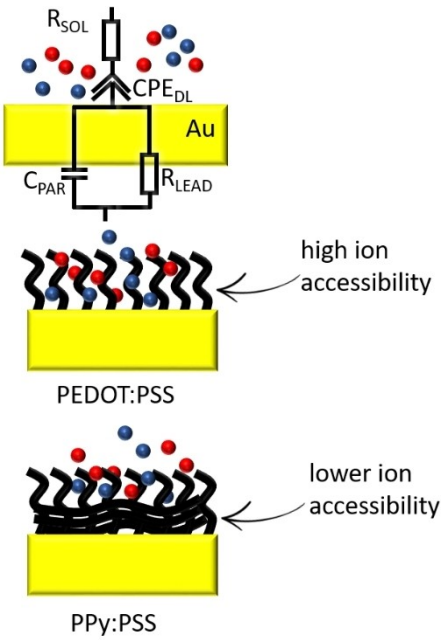

Fig. 6. Schematically representation of the surface morphology of an Au electrode with the proposed EEC model (top), a PEDOT:PSS coated electrode (middle), and a PPy:PSS coated electrode (bottom). Furthermore, the ion accessibility is illustrated for the two polymer-coated electrodes. Drawing is not to scale.

Compared to Snook et al. [13] and as a novelty in this publication, we used one universal model to quantify the electrical parameters of electrodes with different PEDOT/PSS co-polymers coatings. The model proposes physically meaningful circuit elements, which are in good agreement with literature values.

4 Conclusion

This study introduced one simple and universal EEC model with only four components to fit EIS spectra of different electrode/electrolyte interfaces over a broad

range of frequencies. The fitting of the EEC matched very closely with the EIS spectra for different types of electrodes. Furthermore, we could show that the model provides reliable results due to the comparison of the parasitic capacitances. For all investigated electrodes, the parasitic capacitance was found to be 1.35 nF (±0.22 nF). Since the same experimental setup was used, a low variation in the parasitic capacitance was expected and proved by our model. Based on our findings, the combination of PEDOT and PPy with PSS exhibited the capacitance $Q(CPE_{DL})$ of a PPy:PSS coated electrode material for low deposition charges, while its capacitance kept increasing with higher deposition charges similar to that of a PEDOT:PSS electrode.

The proposed EEC model has great potential in various applications. For instance, by shortcutting the drain and source contacts of an organic electrochemical transistor (OECT), the double layer capacitance of the transistors gate could be easily determined to characterize such devices or benchmark their performance. This is of particular interest if such OECTs are used in frequency-dependent readouts as in one of our previous studies [25]. Furthermore, the well-known swelling of PEDOT:PSS layers could be investigated and expressed by changes in the physical values of the films. Besides gaining electrical information, the circuit elements of the proposed model can be attributed to meaningful physical parameters of the film and changes during its growth. We expect that this straightforward model will be very useful for other polymeric electrode systems and aid the understanding of the growth mechanisms of all types of polymer-coated electrodes in different geometries and applications.

Acknowledgements

The authors thank the DFG for funding under project no. 391107823 and 440055779. The authors would like to thank Jochen Heiß for his assistance in fabrication and Linda Wetzel for carefully proofreading the manuscript. Open Access funding enabled and organized by Projekt DEAL.

Data Availability Statement

Data available on request from the authors.

References

[1] a) J. Rivnay, S. Inal, A. Salleo, R. M. Owens, M. Berggren, G. G. Malliaras, *Nat. Rev. Mater.* **2018**, *3*, 1–14; b) A. Dodabalapur, L. Torsi, H. Katz, *Science* **1995**, *268*, 270–271.
[2] L. Manjakkal, A. Pullanchiyodan, N. Yogeswaran, E. S. Hosseini, R. Dahiya, *Adv. Mater.* **2020**, *32*, 1907254.
[3] a) M. De Kok, M. Buechel, S. Vulto, P. Van de Weijer, E. Meulenkamp, S. De Winter, A. Mank, H. Vorstenbosch, C. Weijtens, V. Van Elsbergen, *Phys. Status Solidi* **2004**, *201*, 1342–1359; b) S. Reineke, M. Thomschke, B. Lüssem, K. Leo, *Rev. Mod. Phys.* **2013**, *85*, 1245.
[4] a) P. R. Das, L. Komsiyska, O. Osters, G. Wittstock, *J. Electrochem. Soc.* **2015**, *162*, A674; b) J. Killian, B. Coffey, F. Gao, T. Poehler, P. Searson, *J. Electrochem. Soc.* **1996**, *143*, 936.
[5] a) A. S. Pranti, A. Schander, A. Bödecker, W. J. S. Lang, A. B. Chemical, *Sens. Actuators B* **2018**, *275*, 382–393; b) A. Schander, S. Strokov, H. Stemmann, T. Teßmann, A. K. Kreiter, W. Lang, *IEEE Sens. J.* **2018**, *19*, 820–825; c) A. Schander, T. Teßmann, S. Strokov, H. Stemmann, A. K. Kreiter, W. Lang, *2016 38th annual international conference of the IEEE engineering in medicine and biology society (EMBC)* **2016**, pp. 6174–6177.
[6] a) S. T. Keene, C. Lubrano, S. Kazemzadeh, A. Melianas, Y. Tuchman, G. Polino, P. Scognamiglio, L. Cinà, A. Salleo, Y. van de Burgt, F. Santoro, *Nat. Mater.* **2020**, *19*, 969–973; b) Y. Van De Burgt, E. Lubberman, E. J. Fuller, S. T. Keene, G. C. Faria, S. Agarwal, M. J. Marinella, A. Alec Talin, A. Salleo, *Nat. Mater.* **2017**, *16*, 414–418.
[7] a) M. Tintelott, T. Kremers, S. Ingebrandt, V. Pachauri, X. T. Vu, *Sensors* **2022**, *22*, 2999; b) T. Kremers, M. Tintelott, V. Pachauri, X. T. Vu, S. Ingebrandt, U. Schnakenberg, *Electroanalysis* **2021**, *33*, 197–207; c) M. Tintelott, V. Pachauri, S. Ingebrandt, X. T. Vu, *Sensors* **2021**, *21*, 5153.
[8] a) M. Feroz, P. Vadgama, *Electroanalysis* **2020**, *32*, 2361–2386; b) T. Guinovart, G. Valdés-Ramírez, J. R. Windmiller, F. J. Andrade, J. Wang, *Electroanalysis* **2014**, *26*, 1345–1353; c) A. Macagnano, A. Bearzotti, F. De Cesare, E. Zampetti, *Electroanalysis* **2014**, *26*, 1419–1429; d) D. Zane, G. Appetecchi, C. Bianchini, S. Passerini, A. Curulli, *Electroanalysis* **2011**, *23*, 1134–1141.
[9] Y. Liang, A. Offenhäusser, S. Ingebrandt, D. Mayer, *Adv. Healthcare Mater.* **2021**, *10*, 2100061.
[10] a) B.-Y. Chang, S.-M. Park, *Annu. Rev. Anal. Chem.* **2010**, *3*, 207; b) O. M. Filipe, C. M. Brett, *Electroanalysis* **2004**, *16*, 994–1001; c) A. Perrotta, S. J. García, M. Creatore, *Plasma Processes Polym.* **2015**, *12*, 968–979.
[11] M. Revenga-Parra, T. García, F. Pariente, E. Lorenzo, C. Alonso, *Electroanalysis* **2011**, *23*, 100–107.
[12] J. E. B. Randles, *Discuss. Faraday Soc.* **1947**, *1*, 11–19.
[13] G. A. Snook, A. S. Best, *J. Mater. Chem.* **2009**, *19*, 4248–4254.
[14] B.-A. Mei, O. Munteshari, J. Lau, B. Dunn, L. Pilon, *J. Phys. Chem. C* **2018**, *122*, 194–206.
[15] J. Lazar, C. Schnelting, E. Slavcheva, U. Schnakenberg, *Anal. Chem.* **2016**, *88*, 682–687.
[16] A. Lasia, *J. Phys. Chem. Lett.* **2022**, *13*, 580–589.
[17] C. Hsu, F. Mansfeld, *Corrosion* **2001**, *57*.
[18] A. S. Bondarenko, G. A. Ragoisha, *J. Solid State Electrochem.* **2005**, *9*, 845–849.
[19] a) M. J. Schöning, A. Poghossian, *Label-free biosensing. In: Advanced Materials, Devices and Applications*, Vol. 16, Springer **2018**, *16*; b) D. Ende, K. M. Mangold, *Chem. Unserer Zeit* **1993**, *27*, 134–140.
[20] A. V. Volkov, K. Wijeratne, E. Mitraka, U. Ail, D. Zhao, K. Tybrandt, J. W. Andreasen, M. Berggren, X. Crispin, I. V. Zozoulenko, *Adv. Funct. Mater.* **2017**, *27*, 1700329.
[21] a) M. Bianchi, S. Carli, M. Di Lauro, M. Prato, M. Murgia, L. Fadiga, F. Biscarini, *J. Mater. Chem. C* **2020**, *8*, 11252–11262; b) K. Lota, V. Khomenko, E. Frackowiak, *J. Phys. Chem. Solids* **2004**, *65*, 295–301.
[22] G. A. Snook, C. Peng, D. J. Fray, G. Z. Chen, *Electrochem. Commun.* **2007**, *9*, 83–88.

[23] T. Kremers, N. Menzel, F. Freitag, D. Laaf, V. Heine, L. Elling, U. Schnakenberg, *Phys. Status Solidi* **2020**, *217*, 1900827.
[24] X. Cui, V. A. Lee, Y. Raphael, J. A. Wiler, J. F. Hetke, D. J. Anderson, D. C. Martin, *J. Biomed. Mater. Res.* **2001**, *56*, 261–272.
[25] F. Hempel, J. K. Y. Law, T. C. Nguyen, R. Lanche, A. Susloparova, X. T. Vu, S. Ingebrandt, *Biosens. Bioelectron.* **2021**, *180*, 113101.

Received: July 21, 2022
Accepted: September 30, 2022
Published online on ■■, ■■

RESEARCH ARTICLE

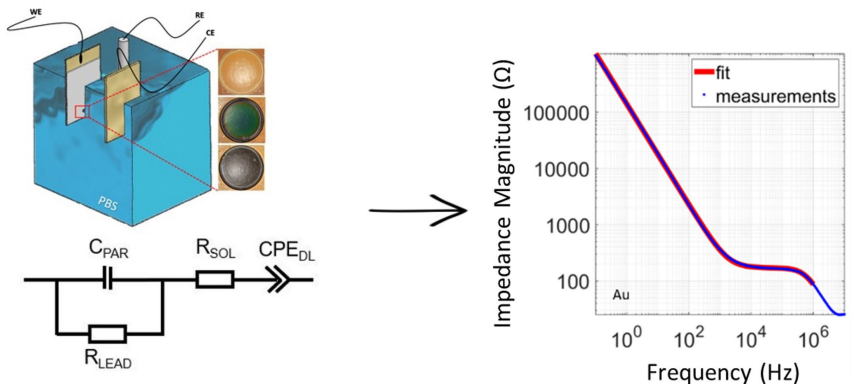

*M. Tintelott, T. Kremers, A. Mernitz, S. Ingebrandt, V. Pachauri, X. T. Vu, U. Schnakenberg**

1 – 9

Physical Interpretation of Mixed Ionic-electronic Conductive Polymer-coated Electrodes by a Simple Universal Impedance Model